OXFORD

Human Molecular Genetics, 2015, Vol. 24, No. 19 5378–5387

doi: 10.1093/hmg/ddv261
Advance Access Publication Date: 10 July 2015
Original Article

ORIGINAL ARTICLE

Novel *POC1A* mutation in primordial dwarfism reveals new insights for centriole biogenesis

Asuman Koparir[1,†], Omer F. Karatas[2,†], Betul Yuceturk[3], Bayram Yuksel[4], Ali O. Bayrak[3], Omer F. Gerdan[3], Mahmut S. Sagiroglu[3], Alper Gezdirici[5], Koray Kirimtay[6], Ece Selcuk[6], Arzu Karabay[6], Chad J. Creighton[7], Adnan Yuksel[9] and Mustafa Ozen[1,8,9,*]

[1]Department of Medical Genetics, Istanbul University, Cerrahpasa Medical School, Istanbul, Turkey, [2]Molecular Biology and Genetics Department, Erzurum Technical University, Erzurum, Turkey, [3]Advanced Genomics and Bioinformatics Research Center (IGBAM), BİLGEM, TUBITAK, Kocaeli, Turkey, [4]Genetic Engineering and Biotechnology Institute, TUBITAK Marmara Research Center, Kocaeli, Turkey, [5]Department of Medical Genetics, Kanuni Sultan Suleyman Training and Research Hospital, 34303 Istanbul, Turkey, [6]Department of Molecular Biology and Genetics, Istanbul Technical University, Istanbul, Turkey, [7]Department of Medicine and Dan L Duncan Cancer Center, Division of Biostatistics and, [8]Department of Pathology and Immunology, Baylor College of Medicine, Houston, TX 77030, USA and [9]Department of Molecular Biology and Genetics, Biruni University, Topkapi, Istanbul, Turkey

*To whom correspondence should be addressed. Tel: +90 2124448222; Fax: +90 2124164646; Email: mozen@bcm.edu

Downloaded from https://academic.oup.com/hmg/article-abstract/24/19/5378/583656 by guest on 06 March 2020

Abstract

POC1A encodes a WD repeat protein localizing to centrioles and spindle poles and is associated with short stature, onychodysplasia, facial dysmorphism and hypotrichosis (SOFT) syndrome. These main features are related to the defect in cell proliferation of chondrocytes in growth plate. In the current study, we aimed at identifying the molecular basis of two patients with primordial dwarfism (PD) in a single family through utilization of whole-exome sequencing. A novel homozygous p.T120A missense mutation was detected in *POC1A* in both patients, a known causative gene of SOFT syndrome, and confirmed using Sanger sequencing. To test the pathogenicity of the detected mutation, primary fibroblast cultures obtained from the patients and a control individual were used. For evaluating the global gene expression profile of cells carrying p.T120A mutation in *POC1A*, we performed the gene expression array and compared their expression profiles to those of control fibroblast cells. The gene expression array analysis showed that 4800 transcript probes were significantly deregulated in cells with p.T120A mutation in comparison to the control. GO term association results showed that deregulated genes are mostly involved in the extracellular matrix and cytoskeleton. Furthermore, the p.T120A missense mutation in *POC1A* caused the formation of abnormal mitotic spindle structure, including supernumerary centrosomes, and changes in POC1A were accompanied by alterations in another centrosome-associated WD repeat protein p80-katanin. As a result, we identified a novel mutation in POC1A of patients with PD and showed that this mutation causes the formation of multiple numbers of centrioles and multipolar spindles with abnormal chromosome arrangement.

[†]These authors contributed equally.

Received: May 11, 2015. **Revised and Accepted:** July 4, 2015

© The Author 2015. Published by Oxford University Press. All rights reserved. For Permissions, please email: journals.permissions@oup.com

Introduction

Primordial dwarfism (PD) is a group of genetically heterogeneous disorders, and the term is used for describing prenatal onset growth failure, which persists postnatally. PD is divided into two groups according to the head circumferences (HCs) of the affected individuals: microcephalic and normocephalic. Microcephaly, associated with reduced brain size, is accompanied with most PD disorders including Seckel syndrome (MIM no. 210600), microcephalic osteodysplastic PD (MOPD) type I (MIM no. 210710) and type II (MIM no. 210720) and Meier–Gorlin syndrome (MIM no. 224690), which were generally related with intellectual disability, except for MOPDII. There are other syndromes such as Cornelia de Lange and Bloom's syndromes, which are characterized by prenatal onset growth retardation and microcephaly; however, patients diagnosed with these syndromes also have other distinctive features. In contrast, a few PD disorders are described with normal HC and usually normal intelligence including 3M syndrome (MIM no. 273750), Silver–Russell syndrome (MIM no. 180860) and Mulibrey nanism (MIM no. 253250). Short stature, onychodysplasia, facial dysmorphism and hypotrichosis (SOFT) syndrome (MIM no. 614813), which was described recently, is incompatible with this classification, as HC is normal in childhood and getting smaller with advancing ages (1).

To date, more than 10 genes have been associated with microcephalic PD. Three of these genes are as follows: *PCNT*, *CENPJ* (synonym with *CPAP*) and *CEP152*, which are related to centrosomal functions (2–4). Although SOFT syndrome is not a microcephalic PD, the only associated gene with this syndrome, *POC1A*, encodes POC1 centriolar protein A, which localizes to centrioles and spindle poles (1). Centrosome integrity and duplication are highly critical for cell cycle as microtubules use centrosomes as anchoring points to extend from both poles in bipolar spindle in order to capture the chromosomes. Therefore, centrosome targeting is the most critical step for correct spindle formation, and given the established role of *POC1A* in centriole formation and maintenance, the gene is expected to have abnormalities in the mitotic spindle in the presence of the deleterious mutations.

Centrosome localization is the primary driving factor for microtubule organization in both interphase and mitotic cells as centrosomes serve as microtubule organization centers, and mutations in centrosome-associated proteins underlie defects in microtubule organization resulting abnormal spindle formation. WD40 microtubule-associated proteins have long been known for their roles in centrosome targeting. In addition to *POC1A*, among many other centrosome-related microtubule-associated proteins is katanin (5). Katanin is a dimeric protein, which consists of p60 and p80 subunits. P60/KATNA1 is a microtubule-severing enzyme that functions in the release of centrosome-born microtubules and regulates microtubule length in both mitotic spindle and non-dividing/interphase cells. P80/KATNB1 is also a WD40 domain protein that binds to p60 as a regulatory subunit and targets p60 to the centrosome to further mediate its interactions with other centrosome-related microtubule-associated proteins.

Shalev *et al.* (1) first described SOFT syndrome in eight patients from two unrelated families in 2012. Since then, only two reports have been published related to this syndrome (6,7). SOFT syndrome is characterized by prenatal onset growth retardation, brachydactyly, onychodysplasia, postpubertal onset hypotrichosis, normal psychomotor development and facial dysmorphisms including dolichocephaly, elongated triangular face, prominent forehead and nose and abnormal ears. Major skeletal findings include short long bones, femoral necks, carpals, metacarpals, tarsals and metatarsals and also vertebral body ossification delay.

In the current study, we utilized whole-exome sequencing (WES) in our PD patients to screen all disease-related and candidate genes to find out the molecular etiology of the syndrome. A novel p.T120A homozygous missense mutation in exon 4 of *POC1A*, which is a causative gene of SOFT syndrome, was detected. The variants were confirmed using Sanger sequencing, and functional analysis of the mutant allele was performed using the fibroblast cells cultured from skin biopsies of the patients. In addition, we tested whether the mutation we identified affects the function of the centrosome during mitosis, and given the seemingly redundant and somewhat similar functions of POC1 and p80-katanin, we aimed at investigating the changes in p80-katanin protein in response to non-functional POC1A protein due to the deleterious mutation in POC1A. We also review SOFT patient studies from the literature and describe additional two Turkish siblings, one of whom had tall vertebral bodies and precocious puberty, which might expand the phenotype.

Results

Subjects

The family has two children who are referred to us for short stature by Endocrinology Department. The mother and father are first-degree cousins (Supplementary Material, Fig. S1). Both pregnancies were uncomplicated, with spontaneous vaginal deliveries at the term. The babies had low birth weight with roughly 1800 g and short length.

The first sibling of the family is 12-year-old female. At the age of 9, she was diagnosed with central precocious puberty and she was treated with Lucrin Depot, a gonadotropin-releasing hormone agonist. Cranial and pituitary magnetic resonance imaging was normal. She had short stature, dolichocephaly, sparse hair, broad-wide forehead, sparse eyebrows and eyelashes, prominent antihelix, large and prominent nose, full lips, large mouth, high-arched palate, prognatism, brachydactyly, nail hypoplasia, prominent heels and pes planus (Fig. 1A–E). Skeletal surveys showed slender long bones and tall vertebral bodies (Fig. 1J–N). When she is referred to us at 9 years, her length, weight and HC were 121 cm (–2 SD), 26.5 kg (25 centile) and 51.7 cm (25–50 centile), respectively. Her length for age and weight for age percentiles were demonstrated in Supplementary Material, Figure S2A and B.

The second sibling is 8-year-old male. His physical examinations were similar with the first child having short stature, dolichocephaly, broad-wide forehead, prominent antihelix, prominent nose, large mouth, high-arched palate, prognatism, brachydactyly, nail hypoplasia, prominent heels and pes planus (Fig. 1A and F–I). Radiographic images revealed slender long bones (Fig. 1O–T). Metabolic screenings, echocardiography, abdominal ultrasonography, ophthalmic and otorhinolaryngological examinations of both patients were normal. His length, weight and HC were 91 cm (–4 SD), 14.5 kg (–3.1 SD) and 49.5 (25 centile) cm, respectively, when first examined at the age of 6.5 years. His length for age and weight for age percentiles were demonstrated in Supplementary Material, Figure S2C and D.

Exome sequencing detected a novel *POC1A* mutation

Exome sequencing was performed on the female affected proband (Supplementary Material, Fig. S1). About 92% of the targeted regions were covered at least four times, and the average sequencing depth of the regions was 60-fold. All variants were filtered according to the distinct criteria indicated in Supplementary

Downloaded from https://academic.oup.com/hmg/article-abstract/24/19/5378/583656 by guest on 06 March 2020

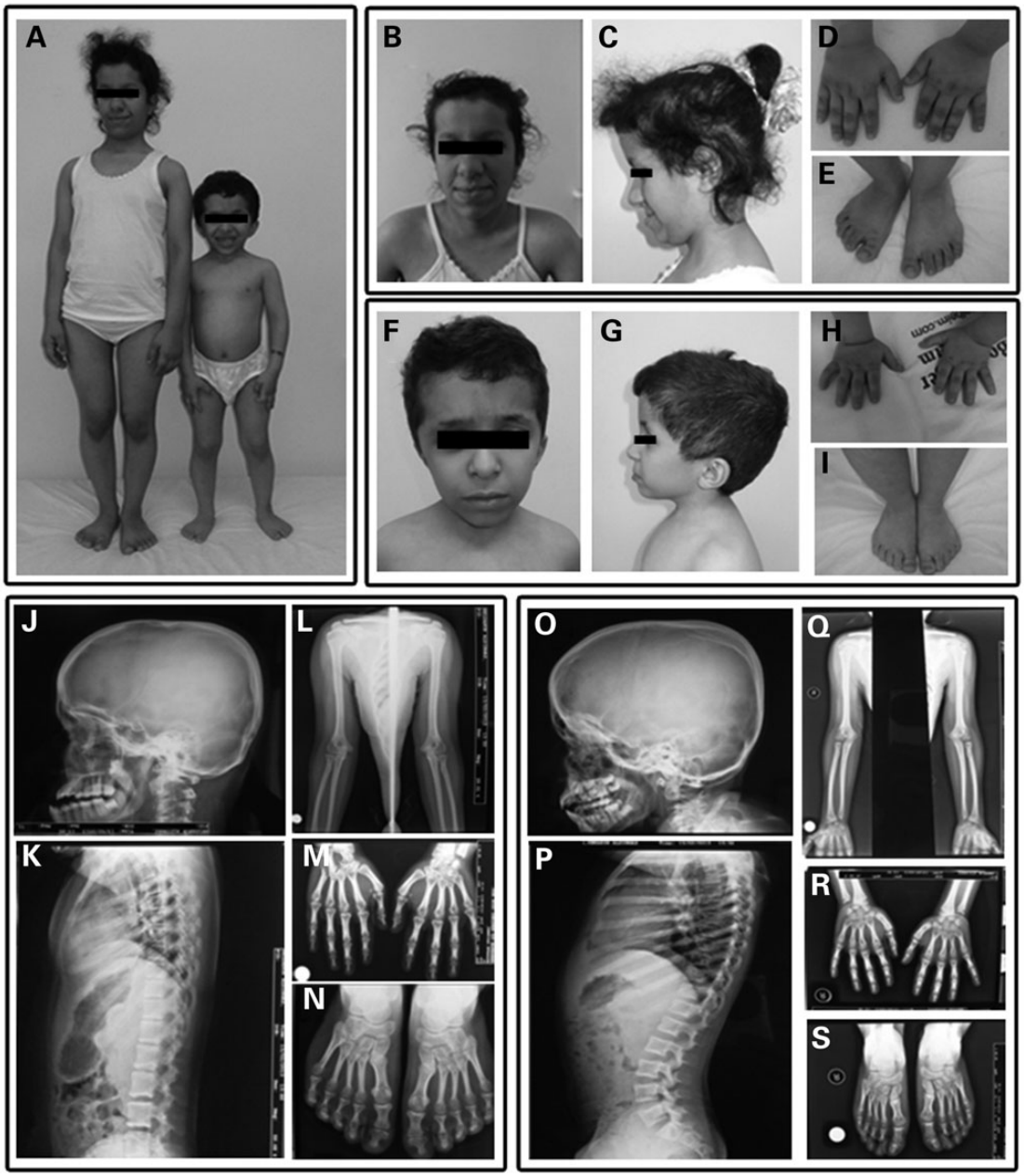


Figure 1. Short stature, dolichocephaly, sparse hair, facial dysmorphism, brachydactyly, nail hypoplasia and pes planus of the first child (**A–E**). Short stature, dolichocephaly, facial dysmorphism, brachydactyly, nail hypoplasia and pes planus of the second child (A and **F–I**). Skeletal surveys of the first child (**J–N**) and second child (**O–S**).

Material, Table S1. Homozygosity mapping results on exome sequencing data, which are produced by HomSI (8), pointed the *POC1A* gene (Supplementary Material, Fig. S2A–D). As a result of WES analysis, we detected a novel p.T120A homozygous missense mutation in exon 4 of *POC1A*, which is a causative gene of SOFT syndrome. To the best of our knowledge, this variation has not been previously reported in the literature and it is not reported in the public databases including Human Genome Mutation Database, 1000 genomes and Exome Variant Server. Sanger sequencing analysis confirmed WES findings in the patient and in her brother and demonstrated that parents are heterozygous carriers for the mutation (Fig. 2A).

In silico analysis demonstrated this novel mutation as deleterious

As to the *in silico* evaluation of the pathogenicity of the detected novel mutation, we initially checked the conservation status of *POC1A* throughout the species. HomoloGene of NCBI database demonstrated that threonine in position 120 resides within a very highly conserved region in *POC1A* (Fig. 2B). Additional testing for pathogenicity of this novel mutation was carried out using different *in silico* tools, all of which indicated the deleterious potential of the amino acid change from threonine to alanine in position 120 (Supplementary Material, Table S2). Furthermore, we

Downloaded from https://academic.oup.com/hmg/article-abstract/24/19/5378/583656 by guest on 06 March 2020

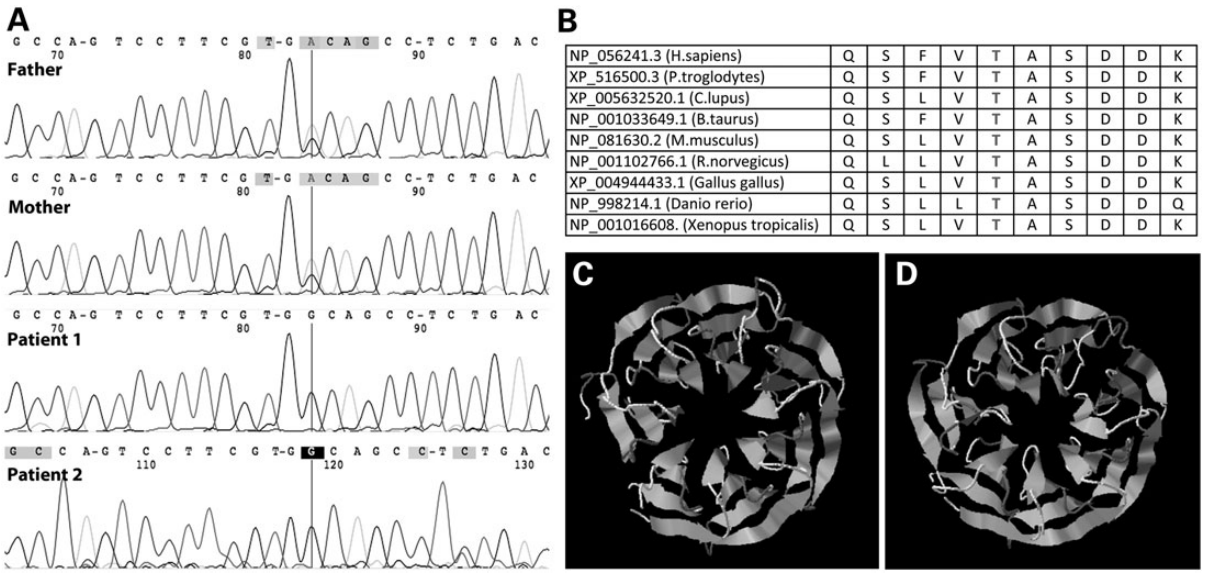


Figure 2. Chromatographs of sequence analysis of *POC1A* in the patients and their parents. (**A**) The conservation status of *POC1A* throughout the species. (**B**) Mutant protein with a conformational change as can be distinguished from the normal protein structure (**C** and **D**).

visualized the theoretical three-dimensional (3D) representation of both wild-type and mutant forms of the POC1A protein, to see any alteration in the structure and conformation of the protein. Our analysis demonstrated that the threonine-to-alanine substitution causes encoding of a misfolded protein (Fig. 2C and D).

Gene expression profiling revealed deregulation of several genes with essential roles in proliferation and cell cycle

To further evaluate the global gene expression profile of cells carrying p.T120A mutation in *POC1A*, we performed the gene expression array and compared their expression profiles with those of control fibroblast cells. The gene expression array analysis showed that 4800 transcript probes were significantly deregulated (fold change >2 for both patients 1 and 2 out of the 45 K gene probes) in cells with p.T120A mutation in comparison to the control. Figure 3A shows the heat-map representation of those 4800 probes (centered each probe on control and sorted them from high- to low-fold change), and top 50 most significantly downregulated and upregulated genes are provided in Supplementary Material, Table S3. GO term association results showed that deregulated genes are mostly involved in the extracellular matrix and cytoskeleton. Figure 3B and C demonstrates the top enriched GO terms for overexpressed and underexpressed genes, respectively. Complete GO term association results are provided as a Supplemental Material file.

Multipolar spindle formation was observed in patient fibroblasts carrying *POC1A* mutation

To study the functional consequence of the *POC1A* pT120A mutation at the cellular level, we used dermal fibroblast culture established from skin biopsies of two patients and control subject. In order to enrich for mitotic cells in culture, cells were synchronized and then immunostained for γ-tubulin antibody for centrosomes, α-tubulin antibody for microtubules and DAPI for chromosomes in order to observe the mitotic spindle in cells. Indeed, we observed multipolar spindle formation and supernumerary centrioles in the mutation-carrying fibroblasts, but not in control cells (Fig. 4). In dividing cells, the mutation affected the mitotic spindle of patient-derived cells displaying disorganized microtubules, and control fibroblast cells showed normal mitotic spindle with organized microtubules (Fig. 4). Patient fibroblasts had abnormal chromosomal alignment among the increased number of centrosomes, and in between centrosomes were chromosomes that were not captured by microtubules in the abnormal mitotic spindles (Fig. 4, patients 1 and 2).

p80-katanin levels increased in both patients

To detect katanin-p80 protein levels in fibroblasts obtained from patients and healthy controls, we performed western blotting (Fig. 5A). Band intensities of p80-katanin were quantified by normalizing, according to the band intensities of β-actin. Then, quantified band intensities were normalized against control samples, and fold changes were calculated (Fig. 5B). The results showed that p80-katanin levels were significantly increased in both patients.

Discussion

Short SOFT syndrome has many overlapping clinical findings with 3M syndrome, Russell–Silver syndrome and Mulibrey nanism, which are called as normocephalic PD syndromes. Clinical distinctive features of SOFT syndrome, 3M syndrome, Russell–Silver syndrome and Mulibrey nanism and the clinical features of our patients are summarized in Table 1.

Table 2 demonstrates the clinical findings of our patients reported here and all other SOFT patients from the literature. All these patients had severe pre–postnatal growth retardation, facial dysmorphisms including triangular elongated face, prominent forehead, ear abnormalities, prominent nose and pointy chin, dolichocephaly, brachydactyly and radiological changes including osteopenia, short tubular bones, carpals, metacarpals, tarsals and metatarsals as the main features of the syndrome. These main features are related to the defect in cell proliferation of chondrocytes in growth plate, which were observed in a mouse

Downloaded from https://academic.oup.com/hmg/article-abstract/24/19/5378/583656 by guest on 06 March 2020

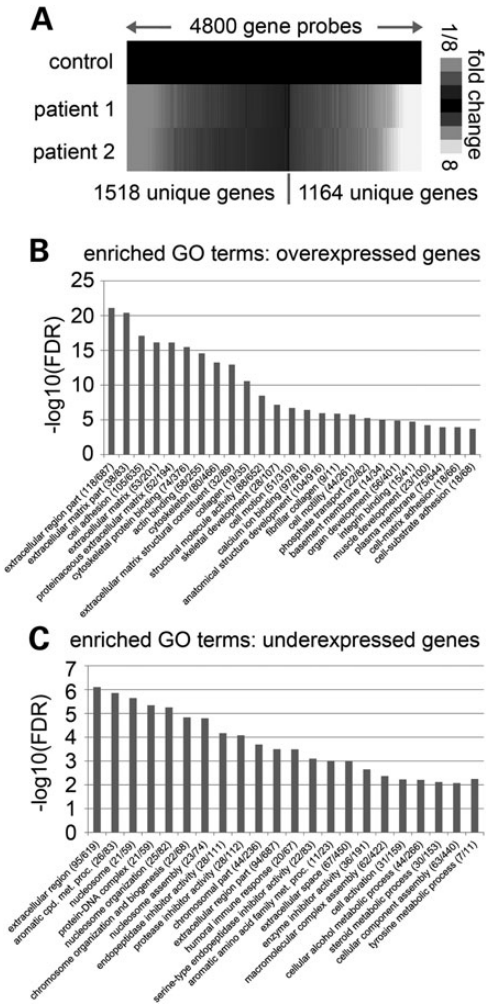


Figure 3. Widespread differences in gene expression, between fibroblast cells with *POC1A* mutation (pT120A) versus control cells. Heat-map representation of differential expression patterns (with each transcript probe centered on control group and with probes sorted from high to low fold change) (**A**). The top enriched GO terms for overexpressed (**B**) and underexpressed genes (**C**).

model (9). Other major clinical findings include hypoplastic nails and postpubertal hypotrichosis. Besides, there are a number of minor clinical findings such as developmental delay and type-2 diabetes. *POC1A* was suggested to be associated with susceptibility to insulin resistance (10); its abnormal function was associated with spermatogenesis defects (9). Therefore, hypogonadism is an important feature of SOFT syndrome, which was observed with elder patients in the literature.

Although vertebral defects such as sagittal clefts were reported in SOFT syndrome, tall vertebral bodies have not been associated with SOFT syndrome before (6,7). Our elder patient had tall vertebral bodies, which is one of the pathognomonic features of 3M syndrome. Because 3M syndrome and SOFT syndrome have many overlapping features, we suggest that SOFT syndrome should be considered in the differential diagnosis of 3M with lack of mutations in causative genes (*CUL7*, *OBSL1* and *CCDC8*), which necessitates *POC1A* sequencing.

Gonadal abnormalities such as undescendent testis, hypergonadotropic hypogonadism, oligo-azoospermia and delay in secondary sex characteristics were reported (6), but in contrast our elder patient had precocious puberty, which was not reported with SOFT syndrome before.

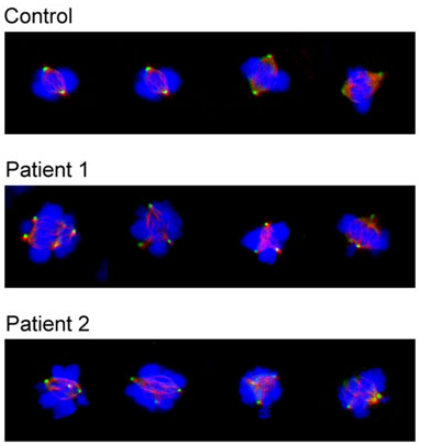


Figure 4. Fibroblast cells obtained from controls and patients were synchronized in mitosis by treatment with 4 mM thymidine and 40 ng/ml nocodazole to arrest in S phase of cell cycle and pre-anaphase of mitosis. Then cells were fixed and stained red with γ-tubulin (green), α-tubulin (red) and DAPI (blue). Cells were visualized by confocal microscopy with 63× objective. Cells were chosen from different areas of control (**A–D**), patient 1 (**E–H**) and patient 2 (**I–L**) samples. Patients' cells show considerable amplification of centrosome number (more than two per cell) and disorganization of microtubules and abnormal chromosomal arrangement compared with control cells.

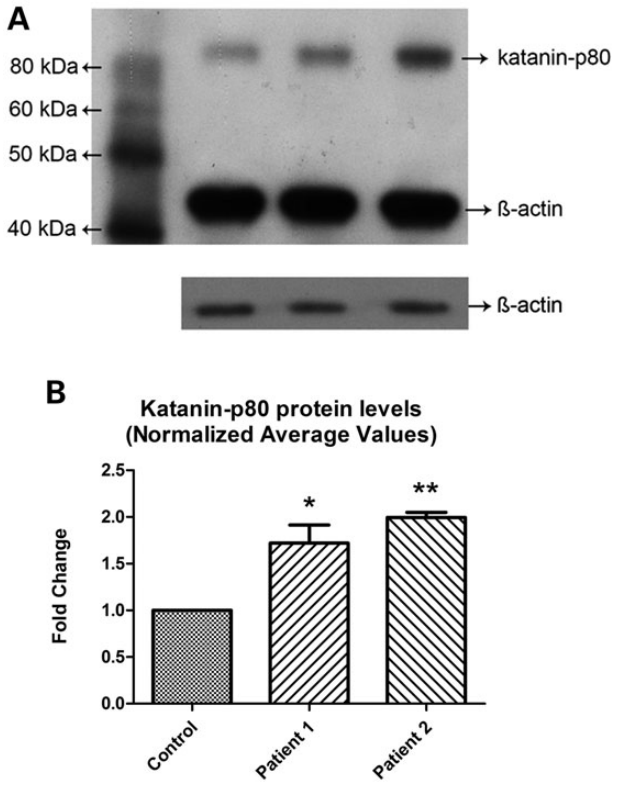


Figure 5. Western blot analysis of p80-katanin in fibroblast obtained from patients and healthy controls. (**A**) Western blot analysis of p80-katanin protein levels. Total protein was extracted from fibroblasts and katanin-p80 levels were observed by using anti-katanin-p80 antibody. Anti-actin antibody was used as loading control. The lower section indicates less-exposed bands of β-actin. Marker was indicated with molecular weights. (**B**) Quantification of western blot image represented in (A). Quantifications were obtained by normalizing band intensities of p80-katanin to those of β-actin (less exposed). Error bars represent ±SD. Asterisk indicates $P<0.05$, showing a statistically meaningful difference.

Downloaded from https://academic.oup.com/hmg/article-abstract/24/19/5378/583656 by guest on 06 March 2020

Table 1. Clinical distinctive features between Russell–Silver, Mulibrey nanism, 3M and SOFT syndromes and presentation of our patient features

	Russell–Silver	Mulibrey nanism	SOFT	3M	Our patients
Inheritance	Isolated cases	AR	AR	AR	AR
Primordial dwarfism	+	+	+	+	+
Head circumference	Normal	Normal	Normal	Normal	Normal
Dolichocephaly	–	+	+	–	+
Triangular face	+	+	+	+/–	+
Frontal bossing	–	+	+	–	+
Limb asymmetry	+	–	–	–	–
Yellow dots on the fundus	–	+	–	–	–
Pericardial constriction	–	+	–	–	–
Vertebral abnormalities	–	–	+	+	+
Prominent nose	–	–	+	–	+
Fleshy tipped nose	–	–	–	+	–
Hypotrichosis (postpubertal)	–	–	+	–	+

We further investigated the global gene expression profile in fibroblast cells, cultured from skin biopsies of p.T120A mutation-carrying patients in *POC1A*. Among the differentially expressed genes, there are many implicated in proliferation, cell cycle and many other important cellular processes. For example, low-density lipoprotein-related protein 1 (*LRP1*), which has the lowest expression in mutation-carrying cells compared with control fibroblast cells, has been demonstrated to be essential for cell morphogenesis as a component of the morphogenesis Orb6 network (11). It also plays critical roles in vasculature through regulating connective tissue growth factor protein levels (12) and in the differentiation of neural stem cells toward oligodendrocytes (13). Another strongly downregulated gene in our patients' fibroblast cells is golgi auto-antigen, golgin subfamily a, 3, *GOLGA3*, which is a golgi complex-associated protein implicated in particularly positioning of the golgi and spermatogenesis. In mice models, lack of Golga3 expression has been reported to interrupt spermatogenesis in late meiosis during the first wave of sperm formation (14). In contrast, caveolin 1, *CAV1*, is one of the most strongly upregulated genes in the fibroblast cells of our patients in comparison to that of control fibroblast cells. *CAV1* is suggested as a tumor suppressor gene whose *in vivo* expression is associated with growth delay, features of muscular differentiation and increased cell death (15). Having increased expression in our patients, it might be speculated as contributing to the disease phenotype. Microtubule-regulating p60-katanin-like protein is also found to be among the strongly upregulated genes in the fibroblast cells of our patients, and the upregulation was much higher in patient 2 compared with that in patient 1. When we further investigated the changes in WD40 repeat protein p80-katanin (*KATNB1*), which is an interacting partner of p60-katanin (*KATNA1*), we also found that the expression was much higher compared with control fibroblast cells, and the increase was more significant in patient 2 (Fig. 5). The clinical phenotype of patient 2 is more severe than that of patient 1 as mentioned in Materials and Methods and presented in Supplementary Material, Figure S2. The katanin upregulation was in accordance with the disorganized microtubules and supernumerary centrioles in the mitotic spindle of patients' fibroblasts as p60-katanin functions in the release of centrosome-born microtubules. As katanin protein functions as a dimer of p60 and p80, the increase in WD40 repeat protein p80-katanin was also expected for compensation of its partner p60-katanin stoichiometrically. p.T120A mutation in the WD40 domain of POC1A is predicted to cause the misfolding of POC1A protein, and therefore the mutation possibly changes POC1A's interaction with its potential partners as the WD40 domain is mainly responsible for protein–protein interactions in multi-protein complex assemblies, in which the repeating units serve as a rigid scaffold for protein interactions. Both being centrosome-related WD40 domain proteins, p80-katanin and POC1A have high homology and we identified that p60-katanin also interacts with POC1A (unpublished data, co-immunoprecipitation) in the same way as it interacts with p80-katanin. Therefore, it might also be possible to speculate that the increased level of WD40 repeat protein p80-katanin might serve to compensate the function of POC1A protein as WD40 proteins are evolutionary conserved. Furthermore, in a recent study, it was shown that the loss of katanin p80 leads to the formation of supernumerary centrioles capable of forming multipolar spindles (16). In this study, we have shown that p.T120A mutation in POC1A also causes the formation of multiple numbers of centrioles forming multipolar spindles with abnormal chromosomal arrangement. It is currently unclear whether the centrosome-associated WD40 proteins have redundant or distinct functions in cells, and multi-protein complex interaction of centrosome-related microtubule-associated proteins remains to be further investigated to understand many human diseases in which a concerted action of centrosomes and microtubules is disrupted.

Materials and Methods

Whole-exome sequencing

Informed consent was obtained from the family. Genomic DNAs were extracted from blood samples of the patients and parents, according to the standard procedures following manufacturer's instructions (Invitrogen, UK). Exonic DNA library was prepared by using Illumina TruSeq Sample Preparation kit and Illumina TruSeq Exome Enrichment kit. Illumina TruSeq PE Cluster Kit v3-cBot-HS was used for paired-end cluster generation, and TruSeq SBS Kit v3-HS reagent kit was used for sequencing the post-capture libraries. Initial clustering was performed on an Illumina cBot machine. Paired-end sequencing was carried out on an Illumina HiSeq 2000 system, with read length of 101. All procedures were performed according to the manufacturer's instructions. Base calling and image analysis were performed using Illumina's Real Time Analysis software version 1.13 with default parameters.

Exome sequence analysis

The paired-end sequence reads were aligned to the human genome (hg19) using Burrows–Wheeler Aligner software (17).

Downloaded from https://academic.oup.com/hmg/article-abstract/24/19/5378/583656 by guest on 06 March 2020

Downloaded from https://academic.oup.com/hmg/article-abstract/24/19/5378/583656 by guest on 06 March 2020

Table 2. Clinical findings of all reported SOFT patients in the literature and our patients

Features	Shaheen *et al.*					Shalev *et al.*								Our patients	
	1	2	3	4	5	1	2	3	4	5	6	7	8	1	2
Gender	Female	Female	Male	Male	Male	Male	Female	Female	Male	Male	Male	Male	Female	Female	Male
Prenatal growth retardation	+	+	+	+	+	+	+	+	+	+	+	+	+	+	+
Birth parameters															
W	−3.9 SD	−3.8 SD	−2.3 SD	−4.1 SD	−3.7 SD	−3.8 SD	−2.7 SD	NR	−4 SD	−3.2 SD	NR	−3.8 SD	−2.8 SD	−4SD	−3.2 SD
H	−4.7 SD	−5.8 SD	−3 SD	NR	NR	NR	−2.2 SD	NR	−4.75 SD	−5 SD	NR	−4.25 SD	−4.2 SD	NR	NR
HC	−2.2 SD	−2.2 SD	Normal	NR	NR	NR	Normal	NR	NR	NR	NR	Normal	−2 SD	NR	NR
Postnatal growth retardation	+	+	+	+	+	+	+	+	+	+	+	+	+	+	+
Growth parameters at recurrent examinations															
Age	6 y	22 m	3.5 m	6 y	32 m	30 y	3 m	33 y	13 m	9 m	8 y	2 m	9 y	9 y	6.5 y
W	−5 SD	−6.3 SD	−3.2 SD	−6.3 SD	−5.9 SD	NR	−2 SD	NR	−5 SD	−6 SD	−6 SD	−5 SD	NR	Normal (25 centile)	−3.1 SD
H	−6.7 SD	−7.1 SD	−5.1 SD	−7.1 SD	−7.1 SD	−7 SD	−2 SD	−9 SD	−6 SD	−6 SD	−4 SD	−5 SD	−8 SD	−2.2 SD	−5 SD
HC	−2.3 SD	NR	Normal	−6.4 SD	−3.3 SD	−3 SD	Normal	−4 SD	−4 SD	−2.5 SD	NR	−2.5 SD	−2.5 SD	Normal (25–50 centile)	Normal (25 centile)
Age							23 y		14 y		24 y	33 m		11.5 y	8 y
W							NR		NR		NR	NR		Normal (10 centile)	−5 SD
H							−6 SD		−6 SD		−7 SD	−7 SD		−4 SD	−6 SD
HC							−3 SD		−4 SD		−3.5 SD	Normal		Normal (25 centile)	Normal (10 centile)
Developmental delay	–	–	–	+	+	–	–	–	–	–	–	–	–	–	–
Dolichocephaly	+	+	+	+	+	+	NR	NR	+	NR	+	+	+	+	+
Facial dysmorphism[a]	+	+	+	+	+	+	+	+	+	+	+	+	+	+	+
Brachydactyly	+	+	+	+	+	+	+	+	+	+	+	+	+	+	+
Hypoplastic nails	NR	NR	NR	NR	NR	+	+	+	+	+	+	+	+	+	+
Hypotrichosis	NR	NR	NR	NR	NR	+	+	+	NR	NR	+	NR	NR	+	–
Gonadal abnormalities	NR	NR	NR	NR	NR	Undescended testis, hypergonadotropic hypogonadism	Hypo-gonadism	NR	NR	NR	Oligo-azoospermia	NR	NR	Precocious puberty	–
Radiological changes	NR	NR	NR	NR	+	+	NR	NR	+	+	+	NR	+	+	+
Others					Hypotonia	Type 2 DM		Severe waddling gate			Type 2 DM			Tall vertebral bodies	

NR, not reported.

[a]Triangular elongated face, prominent forehead, ear abnormalities, prominent nose and pointy chin.

SAMtools (Sequence Alignment/Map) was used for removing polymerase chain reaction (PCR) duplicates (18). After duplication removal, the coverage depth of targeted exome regions was calculated using BED tools (19). About 89% of the targeted regions were sequenced with at least 8-fold coverage, which is sufficient to identify both homozygous and heterozygous variants. Realignment around insertions and deletions (indels) was performed using The Genome Analysis Toolkit v1.6 (GATK) IndelRealigner (20). In order to discover single nucleotide substitutions and small indels, GATK UnifiedGenotyper was run on aligned reads with recommended parameters. Variants with quality score lower than 50 were discarded. Remaining variants were annotated for novelty compared with dbSNP (build 135). The variations on suspected genes were visually inspected by using Integrative Genomics Viewer (21).

Sanger sequence analysis

Sequence analysis of exon 4 of *POC1A* was carried out by using the following primer pairs: 5′-CTCTTGGATGCCTGTCCTTG-3′ and 5′-ACAATGCTCACTTGGCACAG-3′, which produced a 214 bp PCR product, and amplicons were analyzed by direct DNA-sequence analysis. PCR was carried out under standard conditions using 25 ng genomic DNA and Hot-start Taq-DNA Polymerase at 55°C annealing temperature. PCR products were analyzed by electrophoresis on a 2% agarose gel. DNA sequence reaction was performed using BigDye V1.1 (Life Technologies, Carlsbad, CA, USA) and capillary electrophoresis on 3130XL-sequencer (Applied Biosystems). The sequencing data were analyzed using the ENSEMBL sequence ENST00000394970 as reference.

In silico analysis

HomoloGene of NCBI was used to investigate the conservation status of *POC1A* throughout the species (22). Phyre2 (23) and Jmol (24) programs were used to produce 3D representations of the wild-type and mutant forms of protein. SIFT (25), PolyPhen2 (26) and Mutation Taster (27) programs were used to predict the possible effects of mutations on protein function.

Primary fibroblast cell culture

Punch biopsy materials from the skin samples of the two patients and an age-matched control subject were obtained and immediately used for the establishment of primary fibroblast cell cultures. Initially, cells were dissociated with trypsin ethylenediaminetetraacetic acid and cells were plated in T25 cell culture flasks, in which they were grown in RPMI medium (Gibco-BRL, Bethesda, MA, USA) supplemented with 10% fetal bovine serum (FBS) and 1% penicillin streptomycin amphotericin (PSA) at 37°C in a humidified and 5% CO_2 incubator. Cells were trypsinized and passaged when they reached approximately 70% confluency.

RNA isolation, gene expression array and data analysis

Total RNA isolation from 10^6 cells of each sample was performed using TRIzol reagent (Invitrogen, USA), according to the manufacturer's protocol. About 150 ng of total RNA of samples and Agilent General Human Reference RNA were labeled with Cy5 and Cy3, respectively, using 'Agilent Two-Color Microarray-Based Gene Expression Analysis Kit (Low Input Quick Amp Labeling)'. The labeled and amplified RNAs were purified using 'Qiagen's RNeasy Mini Kit', in accordance with the manufacturer's protocols. Purified samples were heat-denatured and hybridized to Agilent Human genome 4X44K arrays (Agilent Technologies, Santa Clara, CA, USA) at 55°C for 17 h. Following posthybridization washes, slide was scanned in an Agilent Microarray Scanner with Surescan High Resolution Technology (Agilent Technologies). Raw data were extracted from scanned image using Feature Extraction v10.7.3.1 (Agilent Technologies) software and analyzed with Bioconductor software (Agilent Technologies). Loess normalization was used to normalize the data. Log2 expression values for each gene were calculated, and genes with 2-fold change in each sample compared with the controls were selected as differentially expressed. Array data have been deposited into the Gene Expression Omnibus under accession number GSE66314.

Cell cycle synchronization and immunocytochemistry

The fibroblast cells of controls and patients were plated at a density of 5×10^4 cells per poly-L-lysine-coated cover slip. After cells were grown to 70–80% confluency, fibroblast cells were treated with 4 mM thymidine for 30 h, washed and released into thymidine-free fresh medium. After 9 h release from S-phase arrest, the cells were incubated with 40 ng/ml nocodazole for 5 h. After nocodazole treatment, the cells were washed to remove nocodazole, and then all cells were fixed with absolute methanol solution for 5 min at −20°C for immunocytochemistry assay. Following fixation, cells were washed with phosphate-buffered saline three times for 5 min and blocked with blocking buffers (10% donkey serum and 10 mg/ml bovine serum albumin in phosphate-buffered saline) for 1 h. Then, the cells were incubated with rat monoclonal anti-α-tubulin antibody (Serotec) in 1:500 and rabbit monoclonal anti-γ-tubulin antibody (Santa Cruz) in 1:500 dilutions overnight at +4°C. Next day, cells were incubated with Alexa Fluor 647 donkey anti-rat secondary antibody and Alexa Fluor 488 donkey anti-rabbit secondary antibody (Cell Signaling) in 1:1000 dilutions for 1 h at 37°C in the dark. Cover slips were then mounted on Mounting Medium (Sigma-Aldrich Corp.) and analyzed with a Leica TCS SP2 SE confocal microscope (Buffalo Grove, IL, USA). In order to determine the expressional values of the target proteins, pixel analysis was used from raw confocal immunocytochemistry images.

Western blotting

The control and patient fibroblast cells were seeded and grown to 70–80% confluency in 75 cm^2 cell culture flasks, and total proteins were extracted from these cells. Equal amounts (10 µg/lane) of proteins obtained from whole cell extract of control and patient samples were separated by sodium dodecyl sulfate–polyacrylamide gel electrophoresis and transferred onto nitrocellulose membrane. Membrane was blocked in 5% skimmed milk powder/TBST (TBS containing 0.1% Tween 20) for 2 h at room temperature and then stained with the following primary antibodies at indicated dilutions overnight at 4°C: rabbit polyclonal anti-katanin-p80 antibody (1:500, Atlas Antibodies) and rabbit monoclonal anti-β-actin (1:1000, Cell Signaling) in 5% skimmed milk powder/TBST. Membrane was then incubated with horseradish peroxidase-conjugated anti-rabbit IgG secondary antibody (1:5000, Cell Signaling) for 2 h at room temperature. Bands were visualized using Super Signal West Femto Chemiluminescent Substrate (Thermo Scientific) and Kodak Medical X-ray Processor.

Integrative pixel analysis

Photoshop CS5 Software was used to analyze the relative intensity of protein bands in western blot images. The intensity value for each protein band was calculated by measuring the

Downloaded from https://academic.oup.com/hmg/article-abstract/24/19/5378/583656 by guest on 06 March 2020

selected band area and pixel values. Obtained values were normalized against those of internal control (β-actin).

Supplementary Material

Supplementary Material is available at *HMG* online.

Acknowledgements

We thank Yiqun Zhang for technical assistance in microarray analysis. We are grateful to the family for participation in this study and other physicians and staff members of Department of Medical Genetics, Cerrahpasa Medical School, Istanbul University, for their involvement in the management of the patients.

Conflict of Interest statement. The authors declare no conflicts of interest.

Funding

This work was supported by the Republic of Turkey Ministry of Development Infrastructure Grant (no. 2011K120020 to B.Y., A.O.B., O.F.G. and M.S.S.) and BILGEM—TUBITAK (the Scientific and Technological Research Council of Turkey) (grant no. T439000 to B.Y., A.O.B., O.F.G. and M.S.S.).

References

1. Shalev, S.A., Spiegel, R. and Borochowitz, Z.U. (2012) A distinctive autosomal recessive syndrome of severe disproportionate short stature with short long bones, brachydactyly, and hypotrichosis in two consanguineous Arab families. *Eur. J. Med. Genet.*, **55**, 256–264.
2. Griffith, E., Walker, S., Martin, C.A., Vagnarelli, P., Stiff, T., Vernay, B., Al Sanna, N., Saggar, A., Hamel, B., Earnshaw, W.C. *et al.* (2008) Mutations in pericentrin cause Seckel syndrome with defective ATR-dependent DNA damage signaling. *Nat. Genet.*, **40**, 232–236.
3. Al-Dosari, M.S., Shaheen, R., Colak, D. and Alkuraya, F.S. (2010) Novel CENPJ mutation causes Seckel syndrome. *J. Med. Genet.*, **47**, 411–414.
4. Kalay, E., Yigit, G., Aslan, Y., Brown, K.E., Pohl, E., Bicknell, L.S., Kayserili, H., Li, Y., Tüysüz, B., Nürnberg, G. *et al.* (2011) CEP152 is a genome maintenance protein disrupted in Seckel syndrome. *Nat. Genet.*, **43**, 23–26.
5. Hartman, J.J., Mahr, J., McNally, K., Okawa, K., Iwamatsu, A., Thomas, S., Cheesman, S., Heuser, J., Vale, R.D. and McNally, F.J. (1998) Katanin, a microtubule-severing protein, is a novel AAA ATPase that targets to the centrosome using a WD40-containing subunit. *Cell*, **93**, 277–287.
6. Sarig, O., Nahum, S., Rapaport, D., Ishida-Yamamoto, A., Fuchs-Telem, D., Qiaoli, L., Cohen-Katsenelson, K., Spiegel, R., Nousbeck, J., Israeli, S. *et al.* (2012) Short stature, onychodysplasia, facial dysmorphism, and hypotrichosis syndrome is caused by a POC1A mutation. *Am. J. Hum. Genet.*, **91**, 337–342.
7. Shaheen, R., Faqeih, E., Shamseldin, H.E., Noche, R.R., Sunker, A., Alshammari, M.J., Al-Sheddi, T., Adly, N., Al-Dosari, M.S., Megason, S.G. *et al.* (2012) POC1A truncation mutation causes a ciliopathy in humans characterized by primordial dwarfism. *Am. J. Hum. Genet.*, **91**, 330–336.
8. Görmez, Z., Bakir-Gungor, B. and Sagiroglu, M.S. (2014) HomSI: a homozygous stretch identifier from next-generation sequencing data. *Bioinformatics*, **30**, 445–447.
9. Geister, K.A., Brinkmeier, M.L., Burgess, D.L., Cavalcoli, J., Cheung, L.Y., Oatley, J.M., Oatley, M., Wendt, J. and Camper, S.A. (2014) Poc1a, a component of the centriole and cilia, causes skeletal dysplasia and male infertility: a mouse model. American Society of Human Genetics Conference, San Diogo, California, USA.
10. Payne, F., Bottomley, W., Isaac, I., O'Rahilly, S., Savage, D.B., Semple, R.K., Barroso, I. and Consortium, T.U.K. (2014) Lessons Learned From the Sequencing of Severe Insulin Resistance Exomes. American Society of Human Genetics Conference, San Diego, California, USA.
11. Kume, K., Kubota, S., Koyano, T., Kanai, M., Mizunuma, M., Toda, T. and Hirata, D. (2013) Fission yeast leucine-rich repeat protein Lrp1 is essential for cell morphogenesis as a component of the morphogenesis Orb6 network (MOR). *Biosci. Biotechnol. Biochem.*, **77**, 1086–1091.
12. Muratoglu, S.C., Belgrave, S., Hampton, B., Migliorini, M., Coksaygan, T., Chen, L., Mikhailenko, I. and Strickland, D.K. (2013) LRP1 protects the vasculature by regulating levels of connective tissue growth factor and HtrA1. *Arterioscler. Thromb. Vasc. Biol.*, **33**, 2137–2146.
13. Hennen, E., Safina, D., Haussmann, U., Worsdorfer, P., Edenhofer, F., Poetsch, A. and Faissner, A. (2013) A LewisX glycoprotein screen identifies the low density lipoprotein receptor-related protein 1 (LRP1) as a modulator of oligodendrogenesis in mice. *J. Biol. Chem.*, **288**, 16538–16545.
14. Bentson, L.F., Agbor, V.A., Agbor, L.N., Lopez, A.C., Nfonsam, L.E., Bornstein, S.S., Handel, M.A. and Linder, C.C. (2013) New point mutation in Golga3 causes multiple defects in spermatogenesis. *Andrology*, **1**, 440–450.
15. Huertas-Martinez, J., Rello-Varona, S., Herrero-Martin, D., Barrau, I., Garcia-Monclus, S., Sainz-Jaspeado, M., Lagares-Tena, L., Nunez-Alvarez, Y., Mateo-Lozano, S., Mora, J. *et al.* (2014) Caveolin-1 is down-regulated in alveolar rhabdomyosarcomas and negatively regulates tumor growth. *Oncotarget*, **5**, 9744–9755.
16. Hu, W.F., Pomp, O., Ben-Omran, T., Kodani, A., Henke, K., Mochida, G.H., Yu, T.W., Woodworth, M.B., Bonnard, C., Raj, G.S. *et al.* (2014) Katanin p80 regulates human cortical development by limiting centriole and cilia number. *Neuron*, **84**, 1240–1257.
17. Li, H. and Durbin, R. (2009) Fast and accurate short read alignment with Burrows–Wheeler transform. *Bioinformatics*, **25**, 1754–1760.
18. Li, H., Handsaker, B., Wysoker, A., Fennell, T., Ruan, J., Homer, N., Marth, G., Abecasis, G. and Durbin, R. (2009) The Sequence Alignment/Map format and SAMtools. *Bioinformatics*, **25**, 2078–2079.
19. Quinlan, A.R. and Hall, I.M. (2010) BEDTools: a flexible suite of utilities for comparing genomic features. *Bioinformatics*, **26**, 841–842.
20. DePristo, M.A., Banks, E., Poplin, R., Garimella, K.V., Maguire, J.R., Hartl, C., Philippakis, A.A., del Angel, G., Rivas, M.A., Hanna, M. *et al.* (2011) A framework for variation discovery and genotyping using next-generation DNA sequencing data. *Nat. Genet.*, **43**, 491–498.
21. Robinson, J.T., Thorvaldsdottir, H., Winckler, W., Guttman, M., Lander, E.S., Getz, G. and Mesirov, J.P. (2011) Integrative genomics viewer. *Nat. Biotechnol.*, **29**, 24–26.
22. Binkley, J., Karra, K., Kirby, A., Hosobuchi, M., Stone, E.A. and Sidow, A. (2010) ProPhylER: a curated online resource for protein function and structure based on evolutionary constraint analyses. *Genome Res.*, **20**, 142–154.
23. Kelley, L.A. and Sternberg, M.J. (2009) Protein structure prediction on the Web: a case study using the Phyre server. *Nat. Protoc.*, **4**, 363–371.

Downloaded from https://academic.oup.com/hmg/article-abstract/24/19/5378/583656 by guest on 06 March 2020

24. Steinbeck, C., Krause, S. and Kuhn, S. (2003) NMRShiftDB—constructing a free chemical information system with open-source components. *J. Chem. Inf. Comput. Sci.*, **43**, 1733–1739.
25. Kumar, P., Henikoff, S. and Ng, P.C. (2009) Predicting the effects of coding non-synonymous variants on protein function using the SIFT algorithm. *Nat. Protoc.*, **4**, 1073–1081.
26. Adzhubei, I.A., Schmidt, S., Peshkin, L., Ramensky, V.E., Gerasimova, A., Bork, P., Kondrashov, A.S. and Sunyaev, S.R. (2010) A method and server for predicting damaging missense mutations. *Nat. Methods*, **7**, 248–249.
27. Schwarz, J.M., Rodelsperger, C., Schuelke, M. and Seelow, D. (2010) MutationTaster evaluates disease-causing potential of sequence alterations. *Nat. Methods*, **7**, 575–576.

Downloaded from https://academic.oup.com/hmg/article-abstract/24/19/5378/583656 by guest on 06 March 2020